

Article

# Coastal Evolution and Relative Sea Level Changes at Psatha (Alkyonides Bay, Greece)

Anna Karkani <sup>1,\*</sup>, Niki Evelpidou <sup>1</sup>, Giannis Saitis <sup>1</sup>, Konstantinos Tsanakas <sup>2</sup>, Hara Drinia <sup>1</sup>, Emmanuel Vassilakis <sup>1</sup>, Efthimios Karymbalis <sup>2</sup> and Dimitrios-Vasileios Batzakis <sup>2</sup>

<sup>1</sup> Faculty of Geology and Geoenvironment, National and Kapodistrian University of Athens, Panepistimiopolis, 15784 Athens, Greece

<sup>2</sup> Department of Geography, Harokopio University, 17671 Athens, Greece

\* Correspondence: ekarkani@geol.uoa.gr

**Abstract:** Geomorphological and sedimentological indicators are often used to reconstruct not only coastal evolution, but also relative sea level changes. In this work, we studied the coastal sediments of Psatha bay (Alkyonides Gulf, Greece) and beachrock outcrops in order to reconstruct the coastal evolution of the area. The drillings analysis included stratigraphy, sediment texture and radiocarbon dating. Detailed mapping of the beachrocks was accomplished using DGPS-GNSS, as well as mineralogical analysis and OSL dating of beachrock samples. The new beachrock index points indicate a sea level that fell by  $0.64 \pm 0.13$  m since  $2200 \pm 210$  years BP and by  $0.95 \pm 0.13$  m since  $4160 \pm 320$  years BP, as a direct result of its location near the uplifting footwall of Psatha fault, suggesting further a rate of tectonic uplift of  $\sim 0.26$  mm/yr for the late Holocene.

**Keywords:** beachrocks; corings; sea level markers; Holocene; Corinth Gulf; tectonics



**Citation:** Karkani, A.; Evelpidou, N.; Saitis, G.; Tsanakas, K.; Drinia, H.; Vassilakis, E.; Karymbalis, E.; Batzakis, D.-V. Coastal Evolution and Relative Sea Level Changes at Psatha (Alkyonides Bay, Greece). *J. Mar. Sci. Eng.* **2023**, *11*, 199. <https://doi.org/10.3390/jmse11010199>

Academic Editor: Gerben Ruessink

Received: 11 December 2022

Revised: 26 December 2022

Accepted: 9 January 2023

Published: 12 January 2023



**Copyright:** © 2023 by the authors. Licensee MDPI, Basel, Switzerland. This article is an open access article distributed under the terms and conditions of the Creative Commons Attribution (CC BY) license (<https://creativecommons.org/licenses/by/4.0/>).

## 1. Introduction

Globally, coastal areas are exposed to various natural hazards. The effects of coastal processes on communities have been highlighted by extreme events such as the earthquake and tsunami in the Indian Ocean in 2004 [1]. The impact of such natural hazards during the last decades has resulted in global public awareness and the intensification of scientific research on coastal hazards and coastal changes [2–5]. The research on past coastal hazards is fundamental for understanding the evolution of the paleo-coastlines [6–8]. Furthermore, the study and recording of environmental changes on coastal areas provides valuable information of past and present conditions and provides a useful tool for coastal evolution and relative sea level (RSL) changes.

The identification and study of paleo-shorelines that are today found uplifted or submerged is the basis for understanding the diachronic trend of the coastline [9–11]. Various sea level markers offer clues for the paleoenvironment, tectonics and the relative sea level (RSL) changes [12–19]. Different sea level markers offer different RSL information in relation to their accuracy or their geochronology potential. The most frequently used sea level markers in the Mediterranean are tidal notches [14–16,20,21], marine terraces [22–26], beachrocks [17,27–31], biological indicators [32–36] and archaeological remains [31,37–39], as well as changes in depositional environments as they are recorded in the stratigraphy of coastal sediments [10,40–43]. The Mediterranean coasts are ideal for the detailed study and recording of RSL changes, as they are characterized by a narrow tidal range and the presence of sea level markers with high precision. In addition, recently, new methodologies and protocols have been used in the Mediterranean [19,28,40,44] that allow the homogenization of data and easier comparison between different regions.

RSL histories have also been useful in reconstructing the evolution of many coastal sectors in the Mediterranean [9,13,17,27,28,31,42,43]. Aucelli et al. [13] reconstructed the RSL changes in Pozzuoli Gulf (Italy) using archaeological indicators and determined a sea level

of  $-4.7/-5.20$  m for the beginning of the first c. BCE and a sea level of  $-3.10$  m at the end of the first c. BCE, which allowed the morpho-evolution of the ancient coastal sector during the last 2.1 ka BP. High-resolution bathymetry along with seismic profiles in offshore areas can also contribute to the recognition of RSL changes, paleo-shorelines and paleogeographic reconstructions [45,46]. Coastal evolution in combination with RSL changes have also been accomplished using uplifted and submerged beachrocks [17,27,28]. In fact, recent studies have shown that beachrocks can be accurate sea level indicators when the mineralogy and morphology of the cement is examined and therefore the spatial relationship between the past shoreline and beachrock formation zone can be determined [17,27–30,41].

In this framework, this study focuses on the coastal zone of Psatha, Alkyonides bay, Greece, a tectonically active area, in order to discuss its evolution and RSL changes. For this purpose, corings were accomplished on the marshy area in the landward part of Psatha coast and beachrocks were mapped and dated with OSL.

## 2. Study Area

The study area, Psatha bay, lies in the eastern end of the Corinth Gulf, and particularly in the Alkyonides Gulf (Figure 1). The Corinth Gulf is an asymmetric tectonic rift, with a length of 110 km, width of 30 km and maximum depth of 900 m, and is characterized by high seismicity. According to GPS data, the Corinth Gulf extension rates reach 10–15 mm/yr in the central part and 6.4 mm/yr in the eastern part of the gulf [47–49].

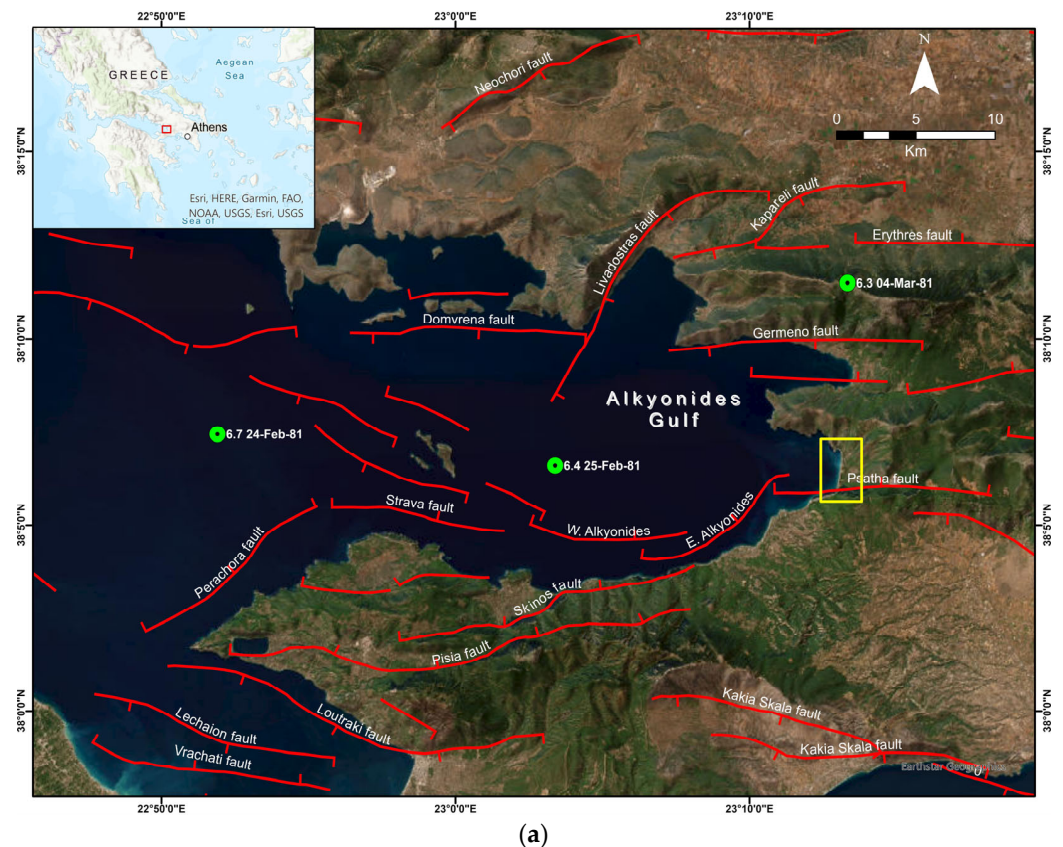
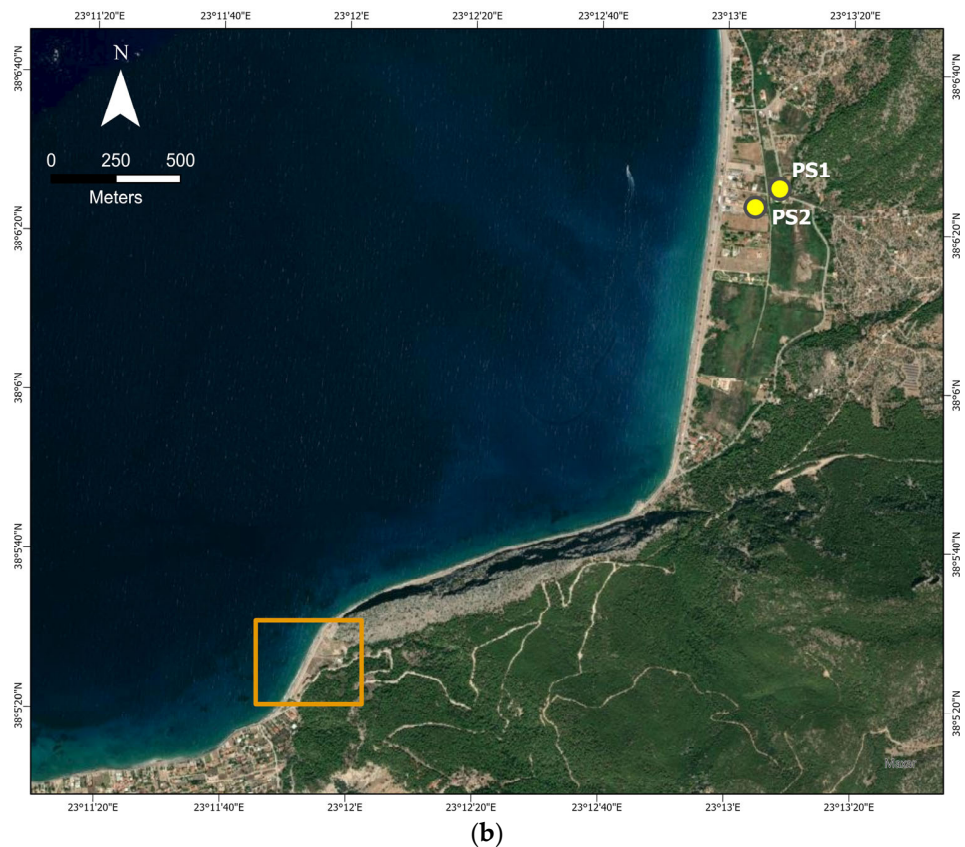


Figure 1. Cont.



**Figure 1.** (a) Tectonic setting of the study area. The yellow box shows the location of the Psatha area. The green circles show the epicenters and magnitudes of the 1981 earthquakes; (b) location of cores PS1 and PS2 and studied beachrocks (yellow box).

The most recent catastrophic earthquakes in the eastern part of the Corinth Gulf occurred in 1981. The earthquake sequence of 1981 included three earthquakes on 24 and 25 February and on 4 March, with magnitudes of  $M = 6.7, 6.4,$  and  $6.3,$  respectively [50,51]. The first two earthquakes ruptured the faults of Pisia and Skinos and the third one the Kapareli fault in the northeast [51,52]. The faults of Pisia and Skinos represent the west and central parts of the south fault system of Alkyonides, respectively, which continue to the west with the fault of Alepochori–Psatha [53]. Numerous active faults, some of which were activated during 1981, control the geomorphology, the morphotectonic structure and the coastal evolution of the area. The study area is bounded by active neotectonic structures that have affected its evolution.

### 3. Materials and Methods

#### 3.1. Coring

In order to reconstruct the coastal evolution of the study area, two boreholes were carried out at the marshy area behind the beach zone of Psatha bay. The marshy area is located in the landward part of the pebble beach of Psatha. The boreholes at shallow depths were drilled with a portable vibracoring sampler (Atlas Corpo Cobra TT) with a diameter of 50 mm. For the paleoenvironmental reconstruction, multiproxy analyses were undertaken, which included sedimentological analysis of the cores, paleontology, and radiocarbon dating. Core PS1 reached 3.96 m in depth and PS2 2.87 m. The precise elevation of the cores was determined using a differential global position system (DGPS) with global navigation satellite system (GNSS) system receiver (Spectra SP60).

The cores were photographed and studied in detail to record the general stratigraphy. The sediment texture was determined by separating out the gravel ( $>2$  mm), sand

(2 mm–63  $\mu\text{m}$ ) and silt/clay (<63  $\mu\text{m}$ ) fractions using two sieve mesh sizes, 2 mm and 63  $\mu\text{m}$ .

The chronostratigraphy of the cores was based on three AMS radiocarbon dates performed at CEntro di DATazione e Diagnostica (CEDAD), in Lecce, Italy. The radiocarbon ages were calibrated through the online software Calib 8.2 [54]. The ages of the shell samples were corrected for the local marine reservoir effect using the MARINE20 curve [55] with a DR value of  $154 \pm 52$  estimated for the Aegean Sea [56].

### 3.2. Beachrocks

#### 3.2.1. Fieldwork and Laboratory Analysis

The spatial mapping of the beachrocks was accomplished using a differential global position system (DGPS) with global navigation satellite system (GNSS) system receiver (Spectra SP60). The detailed recording of the beachrocks included elevation/depth (with respect to the mean sea level), length, and width of the seaward and landward parts with an accuracy of 3 cm. Three transects (S1, S2 and S3) were accomplished, which also included sampling the front (seaward) and the end (landward) of the beachrock slabs [17,28,57].

Samples were collected from the top bed of the beachrocks from both the front and end slabs for microscopic examination. In total, six thin sections were prepared in order to perform petrographic and microstratigraphic analyses. The thin sections were examined through the use of a Leica DMLP (Leica Microsystems GmbH, Wetzlar, Germany) petrographic microscope with a digital camera and the corresponding image treatment software. This allowed us to determine the constituents, the presence of bioclasts and the cement types.

#### 3.2.2. Luminescence Dating

Two beachrock samples were selected (PS-BR1, PS-BR2) for dating by using optically stimulated luminescence (OSL) dating of quartz and were processed at the Luminescence Dating Laboratory of the Institute of Physics, Silesian University of Technology, Poland. For both samples, the luminescence measurements were performed on quartz grains of 125–200  $\mu\text{m}$  in size. A germanium spectrometer was used to determine the radioactivity dose rate. The determination of the equivalent dose was measured with the single aliquot regeneration protocol (OSL-SAR).

### 3.3. Relative Sea Level Reconstruction

The results of the paleoenvironmental reconstruction of the two cores as well as the beachrocks were used to produce a new suite of Sea Level Index Points (SLIPs), following the most recent protocols [19,58,59]. A SLIP must provide the following information in order to be used: (a) the location of the marker, (b) its age and (c) its elevation corrected for the indicative meaning. The indicative meaning of each SLIP is composed of the indicative range (IR), which is the elevation interval over which a marker is formed, and the reference water level (RWL), which is the midpoint of the IR [58]. This protocol has been used in a number of recent Mediterranean studies [40,41,44,60,61].

For the dated samples, SLIPs are calculated based on the following equation:

$$\text{SLIP}_n = A_n - \text{RWL}_n$$

where  $A_n$  is the altitude of the marker and  $\text{RWL}_n$  is the reference water level for that marker.

The vertical errors for each SLIP included: (a) the indicative range, (b) an error of  $\pm 0.03$  m for the samples altitude and (c) a core stretching/shortening error of 0.15 m [58].

Regarding the beachrocks, the samples that showed intertidal formation were used to produce RSL index points. The cement is crucial for identifying the spatial relationship between the coastline and beachrock formation zone. Mauz et al. [29] noted that the uncertainty can be reduced to half the tidal amplitude when the deposit can be ascribed to the upper (or lower) intertidal zone, while a large error can be avoided if cement rather than the thickness or lateral extent of the deposit is taken into account. The dated beachrock

samples of our study area showed clear intertidal formation based on cement characteristics and therefore an indicative range between the mean high tide (MHT) and mean low tide (MLT) (i.e., 0.26 m; HNHS, 2012) was adopted [28,29].

#### 4. Results

##### 4.1. Depositional Environments of Psatha Cores

Core PS1 reached the depth of 3.96 m below the ground level (−2.4 m below sea level) (Figure 2). From 3.96 m to 3.3 m, the core is composed of pebbles mixed with coarse sand of a yellow color at the upper part and gray at the lower part. Gravels represent 80.1% of the total sediment texture, sands 18.5% and silts/clays 1.4%. From 3.3 m to 3.16 m, brown coarse sand is predominant with some broken gastropods. Sands represent 74.5% of the total sediment texture at the top part and gravels reach 22.2%. Between 3.16 m and 3 m, the core consists of pebbles and a few cobbles, most of which are angular. Gravels represent 85.3% of the total sediment texture, sands 13.6% and silts/clays 1.1%. Radiocarbon dating of a marine shell at 3.16 m provided an age of  $705 \pm 45$  BP. This deeper sample yielded an age younger than the other, shallower sample (Table 1).

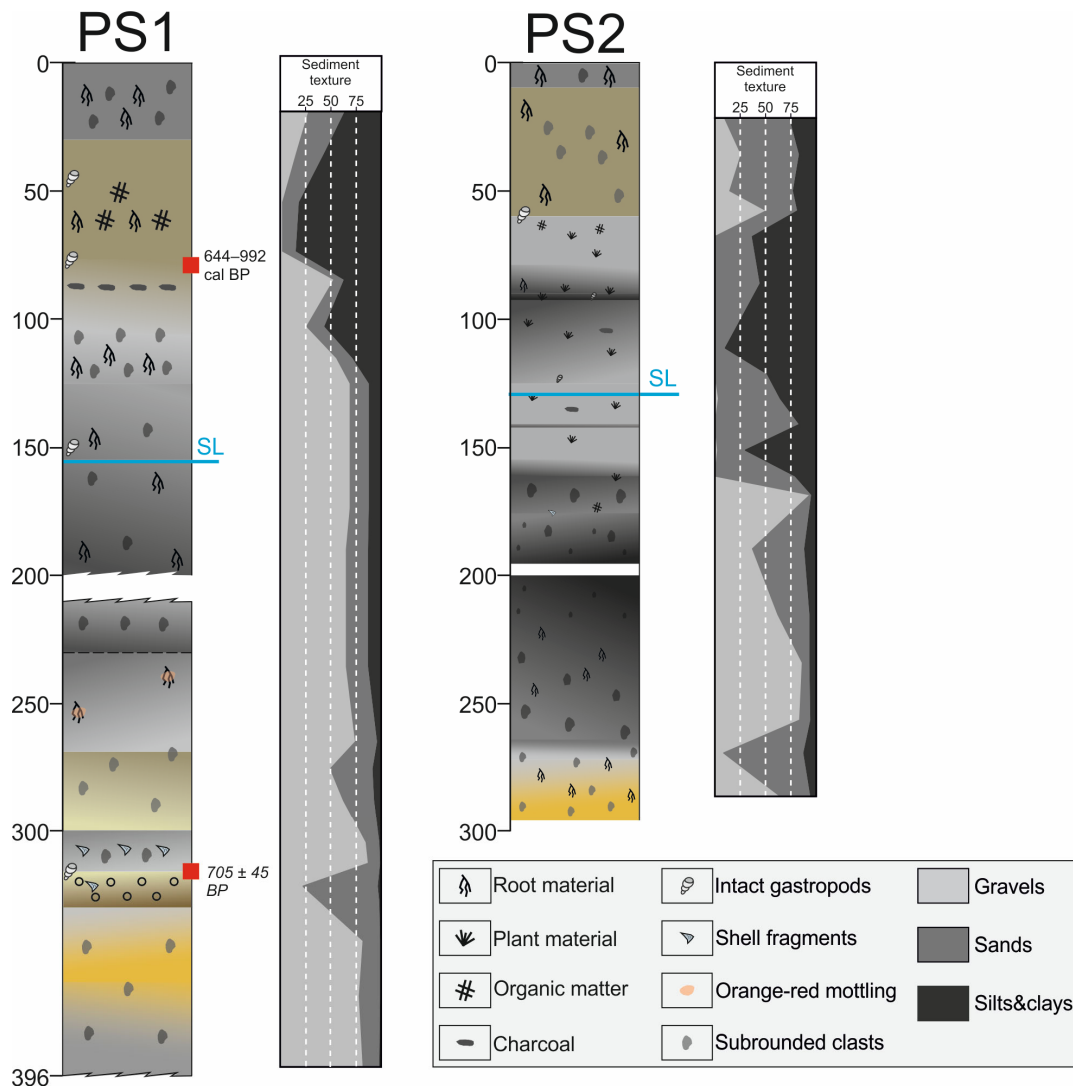


Figure 2. Stratigraphy and radiocarbon dating of PS1 and PS2 cores.

**Table 1.** Radiocarbon ages for dated samples from Psatha cores.

Sample Code	Lab Code	Elevation (m msl)	<sup>14</sup> C Age	Age cal. BP	Cal. BC/AD (2σ)
PS1_G1	LTL22003	+0.79	1584 ± 45	644–992	958–1306 AD
PS1_G2	LTL22004	−0.06			
PS1_G3	LTL22005	−1.6	705 ± 45	-	-

From 3 m to 2.7 m, the stratigraphy is dominated by pebbles mixed with coarse sand of a beige brown color. Gravels represent 55% of the total sediment texture, sands 37% and silts/clays 8%. Between 2.7 m and 2.3 m, the core is composed of pebbles mixed with sand of a gray color. Angular pebbles are more common than rounded ones, while root material is dispersed. Gravels comprise 73.7% of the total sediment texture, sands 22.4% and silts/clays 3.9%. From 2.3 m to 1.25 m, the core consists of dark gray fine sediments mixed with well-rounded clasts. Cobbles are also present sporadically. Gravels compose 67.1% of the total sediment texture, sands 20.3% and silts/clays 12.6%.

Between 1.25 m and 1.06 m, the core is composed of gray fine sediments mixed with subrounded clasts. The presence of gravels in the total sediment texture reaches 55% in the top part, silts/clays reach 28.3% and sands 16.8%. Between 1.06 m and 0.77 m, the core is composed of grayish brown fine sediments with the presence of oxidized roots. In the top part, gravels comprise 53% of the total sediment texture, sands 10.3% and silts/clays 36.6%, while in the lower part, silts/clays increase to 55.8% and gravels decrease to 25.7%. Between 0.77 m and 0.30 m, the core is composed of brown fine sediments with the presence of root material and organic material in its bottom part. The silts/clays fraction comprises 83% of the total sediment texture, sands 14.9% and gravels only 1.8%. Radiocarbon dating at 0.77 m provided an age of 644–992 cal BP (958–1306 AD). The top part (0 to 0.30 m) consists of brown fine sediments, with the presence of roots and clasts. Gravels comprise 27.3% of the total sediment texture, sands 35.8% and silts/clays 36.8%.

Overall, the PS1 core is barren of foraminiferal or ostracod content. The stratigraphy and sediment texture of the core most likely suggests the presence of a low-energy environment that is occasionally influenced by fluvial processes.

Core PS2 reached the depth of 2.87 m below the ground level (−1.58 m below sea level). From 2.87 m to 2.7 m, the core is composed of yellow coarse sand with sub-rounded pebbles. Gravels represent 64.2% of the total sediment texture, sands 30.6% and silts/clays 5.2%. From 2.7 m to 2.6 m, the stratigraphy consists of gray coarse sand with rounded pebbles. Gravels represent 8% of the total sediment texture, sands 80% and silts/clays 12%. From 2.6 m until 2.25 m, the core is composed of pebbles mixed with fine-grained material of a dark gray color. Gravels represent 84.7% of the total sediment texture, sands 9.6% and silts/clays 5.7%. Between 2.25 m and 1.62 m, the stratigraphy consists mainly of sand with pebbles of a dark gray color, with the occasional presence of shell fragments. Cobbles are also present. Gravels represent 64.3% of the total sediment texture, sands 28.4% and silts/clays 7.3%. Between 1.62 m and 1.25 m, the core is composed of fine gray sediments, with sands and silts/clays prevailing, and the sporadic presence of plant remains. From 1.25 m to 0.6 m, the core is composed of fine sediments of a gray color that become progressively darker at the lower part. Sands represent 40.4% of the total sediment texture and silts/clays 59.6% on the upper part, with the latter increasing towards the lower part. Between 0.6 m and 0.1 m, the stratigraphy consists of brown fine sediments, with the presence of roots and sub-rounded pebbles. Sands represent, on average, 60.7% of the total sediment texture, gravels 39.6% and silts/clays 19%. The top 0.1 m of the core is composed of fine sediments with roots.

Overall, the PS2 core is barren of foraminiferal or ostracod content. The stratigraphy and sediment texture of PS2 is similar to PS1, with the presence of a low-energy environment occasionally influenced by fluvial processes.

#### 4.2. Beachrock Morphology and Microstratigraphy

The detailed spatial mapping of Psatha beachrock showed the presence of one outcrop that is developed parallel to the present coastline. The beachrock slab width varies along the coast between 5 and 8 m. Its present-day elevation is between the sea level and +1.1 m (Figures 3 and 4).

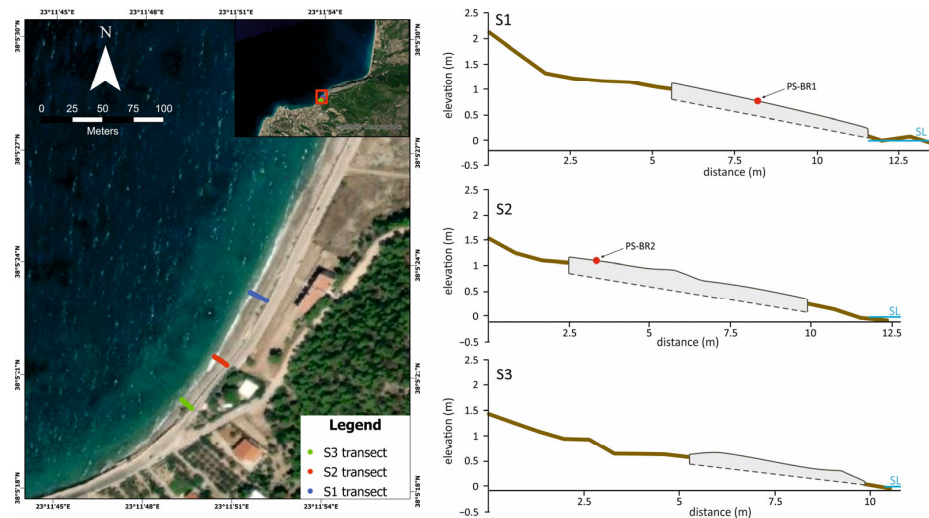


**Figure 3.** Location of the three transects performed on the beachrock slabs on the left figure. On the right is the schematic representation of beachrock cross sections and OSL sample points (red circles).



**Figure 4.** South (a) and north (b) view of the beachrock outcrop of Psatha.

The microscopic observations of the beachrock samples showed a coherent pattern with sub-rounded to well-rounded and well- to moderately sorted grains. The presence of bioclasts reaches about 15%. The lithoclasts are mainly composed of quartz, calcite, pyroxenite and serpentine. Micritic high magnesium calcite (HMC) cement was the most dominant in all samples (Figure 5). The observed bounding material between the grains is mostly middle intertidal cement at the marine phreatic mixing water zone in all samples. The cement forms a thin isopachous coating around the sediment grains as well as pellet forms (e.g., samples S2E and S3E). On the other hand, sample S1E showed a thicker isopachous cement coating, while bladed crystals of HMC and spar were present. In samples S1F, S2F and S3F, the cement forms a more coherent coating as pore filling of a brown color. The cement thickness in the majority of the samples is around 15  $\mu\text{m}$ . Cements of the middle intertidal zone are associated with detrital constituents (rock and bioclasts), which are all present in all samples. Furthermore, the cement micritic crystals forming isopachous micritic coating further indicates intertidal zone beachrock formation. In the above samples, there was absence of meteoric cement. All of the aforementioned

observations allowed us to determine the formation zone of the dated beachrocks within the intertidal zone.

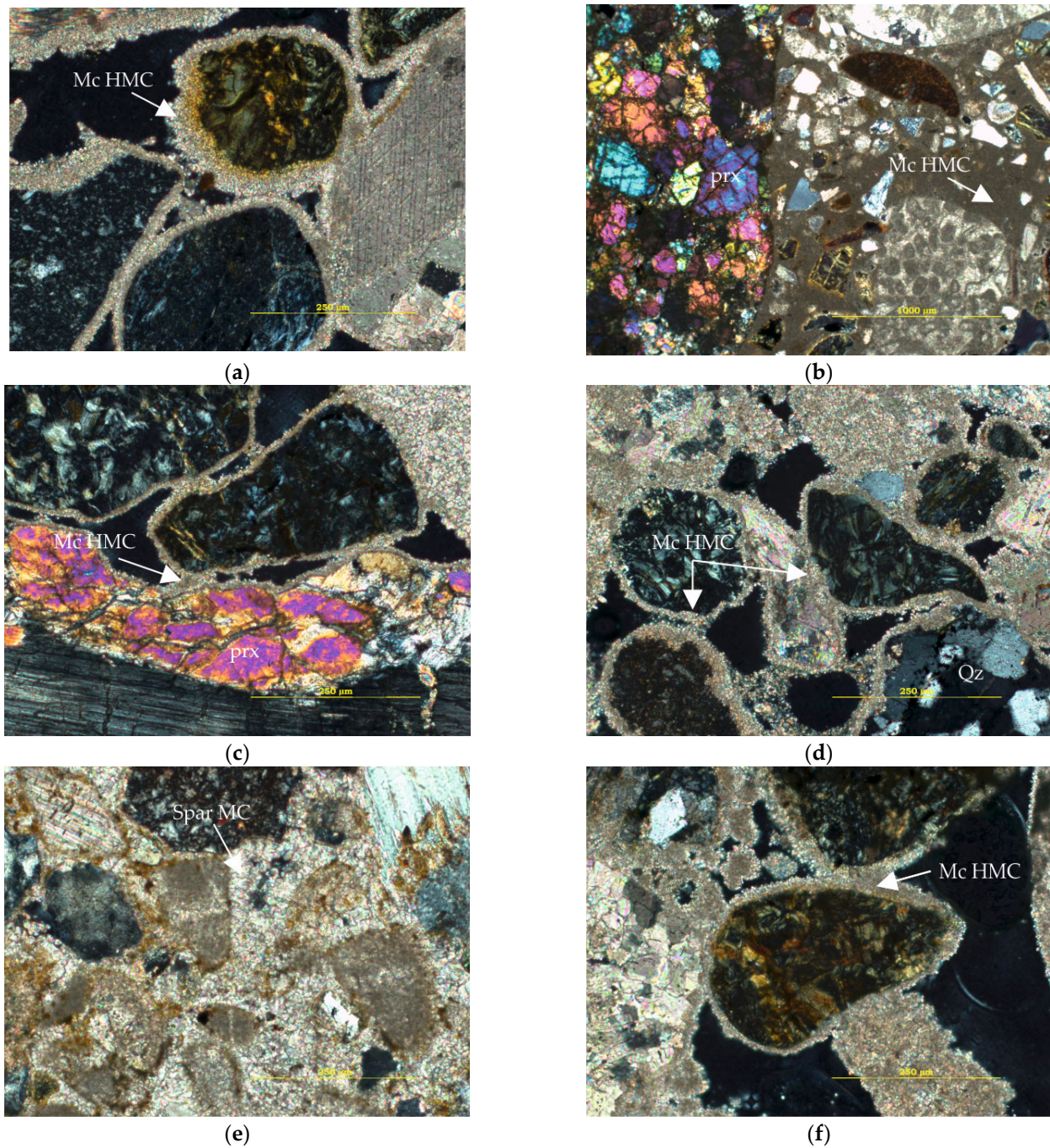


**Figure 5.** Representative photomicrographs under crossed polars illustrating beachrock composition. The photomicrographs are taken from polished thin sections of beachrock samples where Mc: microcrystalline or micritic cement, HMC: high magnesium calcite cement, MC: magnesium calcite, Qz: quartz, prx: pyroxene. Microcrystalline cement with a light brown color is indicative of HMC coating. (a) Thick microcrystalline HMC cement coats lithoclasts and minerals in sample S1E, (b) micritic HMC cement is developed playing the role of pore filling in sample S1F, (c) thick microcrystalline HMC cement coats lithoclasts and minerals in sample S2E, while in (d), thick microcrystalline HMC cement binds grains while forming pore-filling forms in sample S2F. (e) Well-developed sparitic crystals of MC filling all beachrocks pores in sample S3E and (f) thick microcrystalline HMC cement coats lithoclasts while forming pellets and pore-filling forms in sample S3F.

### 4.3. RSL Reconstruction

The two beachrock samples were used as SLIPs based on the cement observations and the OSL dating results (Table 2). Sample PS-BR1 was collected from +0.77 m elevation and provided an age of  $2.20 \pm 0.21$  ka, while sample PS-BR2 was collected from +1.08 m and provided an age of  $4.16 \pm 0.32$  ka. Both samples were converted into SLIPs, suggesting a former sea level at  $+0.64 \pm 0.13$  m and  $+0.95 \pm 0.13$  m, respectively.

**Table 2.** Luminescence dating results of the selected beachrock samples.

Sample Number	Elevation (m)	Method	No of Aliquots	Equivalent Dose (Gy)	Age BP (ka)
PS-BR1	0.77	Quartz	19	1.43	$2.20 \pm 0.21$
PS-BR2	1.08	Quartz	11	2.43	$4.16 \pm 0.32$

The radiocarbon results from the cores only provide a terrestrial limiting point. The shell sample collected at +0.79 m above msl provided an age of 644–992 cal. BP (Table 1) and was most likely deposited in a coastal marshy environment.

## 5. Discussion

The study area, Psatha bay, lies at the eastern end of Alkyonides Gulf. The most recent large earthquakes in Alkyonides Gulf are those of 1981. The earthquakes resulted in rockfalls, a small tsunami and significant coastal uplift and subsidence [62,63]. West of Alepochori, subsidence was noted of the order of 0.6 m that flooded up to 50 m of the former coastline [64]. On the shores of Skinos, several researchers noted subsidence of 0.5–0.8 m, while others report 1.2 m and 1.5 m subsidence [65,66]. According to Jackson et al. [48], residents of the area noted a tsunami with a height of 1 m, during the main earthquake of 1981, which was probably owed to submarine landslides (e.g., [67]).

The landscape and RSL trend of the southern shore of the Alkyonides Gulf is dominated by the activity of the major active normal faults of Skinos, East Alkyonides and Psatha (Figure 1). The new beachrock index points indicate a sea level that fell by  $0.64 \pm 0.13$  m since  $2200 \pm 210$  years BP and by  $0.95 \pm 0.13$  m since  $4160 \pm 320$  years BP. These data suggest a rate of tectonic uplift of  $\sim 0.26$  mm/yr on average. The beachrock site is located near the uplifting footwall of the Psatha fault (Figure 1). Along the base of the limestone cliff of the fault footwall, the presence of three well-developed uplifted notches has been noted by several researchers [68,69], with the upper one reaching an elevation of +1.5–2 m. Due to the construction of the coastal road, these notches are no longer accessible or visible. Although none of the notches have been dated because of their proximity to the studied beachrocks, it is likely that the age of the upper notch is greater than  $4160 \pm 320$  years BP. According to Collier et al. [69], the upper notch began to form about 7000 years ago and estimated an uplift rate of about 0.3 mm/yr. Leeder et al. [70] reported new evidence of footwall uplift in an accumulation of raised beach gravels, with the highest position of this gravel bed at +10.2 m above mean sea level. According to the authors, the youngest plausible age for its formation is MIS 5a at  $\sim 83,000$  years BP, considering a sea level at about  $-10 \pm 4$  m, thus estimating a mean footwall uplift of  $0.24 \pm 0.05$  mm/yr. These estimations are in good agreement with the beachrock elevation and chronology data of our study.

These results are an addition to the recent studies that have used beachrocks as accurate sea level indicators. There has been considerable debate at which position of the tidal zone beachrocks are formed [71]; however, many recent publications have used beachrocks as sea level indicators with good accuracy, which were based on geomorphological, sedimentological and cement microstratigraphy observations. The detailed review by Vousedoukas et al. [72] clarified that the cement is crucial for identifying the spatial relationship between the coastline and beachrock formation zone, while later, Mauz et al. [29] noted that the uncertainty can be reduced to half the tidal amplitude when the beachrock can be ascribed to the upper (or lower) intertidal zone. The cement mineralogy and morphology of the

beachrocks are indicative of the diagenetic environment and large errors can be avoided when this is considered instead of the beachrock thickness or lateral extent [29].

In terms of beachrock chronology, our work suggests that OSL can be a good chronological tool. In general, obtaining a precise age for the formation of beachrocks is a difficult task. Radiocarbon dating has frequently been used to date either bioclasts incorporated in the beachrock or cement. However, well-cemented beachrocks may have undergone many diagenetic phases and therefore dating the cement from one deposit may produce different ages. On the other hand, the dating of biogenic material can only provide a maximum age, considering the time gap between the death of the organism and its incorporation into the beachrock. OSL is increasingly used to date beachrocks and additionally, although most beachrocks are characterized by the high presence of bioclasts, Psatha beachrocks were composed of a little amount. Furthermore, in order to date a bioclast and correspond to the age of a beachrock formation, it should show a high degree of preservation, which would suggest a very short permanence of the dead bioclast on the beach prior to the fossilization within the beachrock formation.

Although the beachrocks cannot offer information on the mode of relative sea level changes (co-seismic or long-term), their present-day elevation reveals that the area has been uplifted by  $0.64 \pm 0.13$  m since  $2200 \pm 210$  years BP and by  $0.95 \pm 0.13$  m since  $4160 \pm 320$  years BP. Given the active tectonics and recent seismicity of the wider area, the uplifted features owe their position today to a combination of seismic events and gradual long-term uplift.

Further south of Psatha bay, studies on raised marine terraces have reported at least two raised shorelines, between 25 and 35 m and between 6.5 and 13 m [50,68,69]. Leeder et al. [70] reported ages of  $90 \pm 4$  ka and  $126 \pm 6$  ka, respectively, for the highest raised marine deposits between 25 and 35 m and correlated them with Marine Isotope Stage 5 (MIS5). By adopting 126 ka as the maximum age, corresponding to MIS5e, they estimated a mean uplift rate of  $\sim 0.3$  mm/yr.

Conversely, the coring site at the coastal marshy area lies in the hanging wall of Psatha fault and is directly related to the subsidence of the hanging wall. Although the radiocarbon results did not allow the production of SLIPs from the cores, the interpretation of depositional environments may provide a general overview. Both cores have similar stratigraphy and sediment texture, lacking any micropaleontological content, such as ostracods and foraminifera. Based on our findings, the presence of a marshy area is suggested, which is occasionally influenced by the fluvial processes of nearby streams. It appears that the study area has not undergone significant changes during the period considered. Furthermore, the lack of paleontological content may suggest that no water circulation occurred at the studied site and that anoxic conditions prevailed (e.g., [73,74]).

Recent RSL studies from the eastern Mediterranean indicate a general RSL rise trend. Evelpidou et al. [66] report an average rate of  $\sim 0.8 \pm 0.2$  mm/yr since  $\sim 5700$  cal BP for Samos Island, in the eastern Aegean. Karkani et al. [28] report a RSL rise by  $\sim 2$  m in the last 2000 years, and by at least  $\sim 3.9$  m since  $\sim 4500$  years BP and estimated a tectonic subsidence for the central Cyclades close to  $1.0 \pm 0.4$  mm/yr since 5500 cal BP. Dean et al. [67] report an RSL from  $0.8 \pm 0.5$  m at  $\sim 2750$  years BP to  $0.0 \pm 0.1$  m by  $\sim 1850$  years BP, with a rate of 0.8 mm/yr for the stable Israel coasts. Conversely, a fall in RSL characterizes areas of tectonic uplift with variable rates ranging from 0.3 mm/yr for southeast Crete [75], 0.36 mm/yr for southeast Peloponnese [25] to 1–1.5 mm/yr in northwest Euboean Gulf [24]. It should be noted that glacial isostatic adjustment (GIA) modeling is frequently added in RSL studies to better quantify the tectonic component [19,41,44,60]. Research frequently uses curves produced by Lambeck et al. [76]; however, such models are continuously updated significantly, and generalized curves are not representative for specific sites and could lead to misleading quantifications.

## 6. Conclusions

In this work, we investigated the evolution of the coastal zone of Psatha bay, Alkyonides Gulf. The main findings may be summarized as follows:

- The combination of coastal sediments, beachrocks, mineralogical and microscopic analysis and OSL dating has shown that the two sites lying in the footwall and hanging wall of Psatha fault, correspondingly, are directly affected by these tectonic features.
- The Psatha coastal marshy area is directly related to the subsidence of the hanging wall of the Psatha fault. It has not undergone significant changes during the period considered, as it is characterized by the presence of a marshy area occasionally influenced by the fluvial processes of nearby streams.
- The microscopic observations of the beachrock samples showed that HMC cement was the most dominant in all samples, characterized as middle intertidal cement at the marine phreatic mixing water zone.
- The beachrocks have uplifted by  $0.64 \pm 0.13$  m since  $2200 \pm 210$  years BP and by  $0.95 \pm 0.13$  m since  $4160 \pm 320$  years BP. Their present-day elevation is linked with their location near the uplifting footwall of the Psatha fault.
- Based on our results, we deduce a rate of tectonic uplift of  $\sim 0.26$  mm/yr for the late Holocene, which is in good agreement with other studies in the wider area.
- Our results highlight the usefulness of beachrocks as RSL proxies when geomorphological, sedimentological and cement microstratigraphy observations are combined.

**Author Contributions:** Conceptualization, A.K. and N.E.; formal analysis, A.K., G.S. and K.T.; writing—original draft preparation, A.K.; writing—review and editing, A.K., N.E., G.S., H.D., E.V., K.T., E.K. and D.-V.B.; visualization, A.K.; supervision, N.E. and A.K. All authors have read and agreed to the published version of the manuscript.

**Funding:** This research is co-financed by Greece and the European Union (European Social Fund—ESF) through the Operational Program “Human Resources Development, Education and Lifelong Learning” in the context of the project “Reinforcement of Postdoctoral Researchers—2nd Cycle” (MIS-5033021), implemented by the State Scholarships Foundation (IKY).

**Institutional Review Board Statement:** Not applicable.

**Informed Consent Statement:** Not applicable.

**Data Availability Statement:** The data presented in this study are available on request from the corresponding author.

**Conflicts of Interest:** The authors declare no conflict of interest.

## References

1. Jankaew, K.; Atwater, B.F.; Sawai, Y.; Choowong, M.; Charoentitirat, T.; Martin, M.E.; Prendergast, A. Medieval Forewarning of the 2004 Indian Ocean Tsunami in Thailand. *Nature* **2008**, *455*, 1228–1231. [[CrossRef](#)]
2. Gelfenbaum, G.; Jaffe, B. Erosion and Sedimentation from the 17 July 1998 Papua New Guinea Tsunami. *Pure Appl. Geophys.* **2003**, *160*, 1969–1999. [[CrossRef](#)]
3. Scheffers, A.; Kelletat, D. Sedimentologic and Geomorphologic Tsunami Imprints Worldwide—A Review. *Earth Sci. Rev.* **2003**, *63*, 83–92. [[CrossRef](#)]
4. Chagué-Goff, C.; Andrew, A.; Szczuciński, W.; Goff, J.; Nishimura, Y. Geochemical Signatures up to the Maximum Inundation of the 2011 Tohoku-Oki Tsunami—Implications for the 869 AD Jogan and Other Palaeotsunamis. *Sediment. Geol.* **2012**, *282*, 65–77. [[CrossRef](#)]
5. England, P.; Howell, A.; Jackson, J.; Synolakis, C. Palaeotsunamis and Tsunami Hazards in the Eastern Mediterranean. *Philos. Trans. R. Soc. A Math. Phys. Eng. Sci.* **2015**, *373*, 20140374. [[CrossRef](#)]
6. Karkani, A.; Evelpidou, N.; Tzouxanioti, M.; Petropoulos, A.; Gogou, M.; Mloukie, E. Tsunamis in the Greek Region: An Overview of Geological and Geomorphological Evidence. *Geosciences* **2022**, *12*, 4. [[CrossRef](#)]
7. Evelpidou, N.; Karkani, A.; Polidorou, M.; Saitis, G.; Zerefos, C.; Synolakis, C.; Repapis, C.; Tzouxanioti, M.; Gogou, M. Palaeo-Tsunami Events on the Coasts of Cyprus. *Geosciences* **2022**, *12*, 58. [[CrossRef](#)]
8. Anzidei, M.; Lambeck, K.; Antonioli, F.; Furlani, S.; Mastronuzzi, G.; Serpelloni, E.; Vannucci, G. Coastal Structure, Sea-Level Changes and Vertical Motion of the Land in the Mediterranean. *Geol. Soc. Lond. Spec. Publ.* **2014**, *388*, 453–479. [[CrossRef](#)]

9. Mattei, G.; Aucelli, P.P.C.; Caporizzo, C.; Rizzo, A.; Pappone, G. Morpho-Evolutive Trends and Relative Sea-Level Changes of Naples Coast in the Last 6000 Years. *Water* **2020**, *12*, 2651. [\[CrossRef\]](#)
10. Caporizzo, C.; Gracia, F.J.; Aucelli, P.P.C.; Barbero, L.; Martín-Puertas, C.; Lagóstena, L.; Ruiz, J.A.; Alonso, C.; Mattei, G.; Galán-Ruffoni, I.; et al. Late-Holocene Evolution of the Northern Bay of Cádiz from Geomorphological, Stratigraphic and Archaeological Data. *Quat. Int.* **2021**, *602*, 92–109. [\[CrossRef\]](#)
11. Karymbalis, E.; Tsanakas, K.; Karkani, A.; Evelpidou, N. Tectonics and Sea-Level Fluctuations. *J. Mar. Sci. Eng.* **2022**, *10*, 334. [\[CrossRef\]](#)
12. Chelli, A.; Pappalardo, M.; Bini, M.; Brückner, H.; Neri, G.; Neri, M.; Spada, G. Assessing Tectonic Subsidence from Estimates of Holocene Relative Sea-Level Change: An Example from the NW Mediterranean (Magra Plain, Italy). *Holocene* **2017**, *27*, 1988–1999. [\[CrossRef\]](#)
13. Aucelli, P.P.C.; Mattei, G.; Caporizzo, C.; Cinque, A.; Troisi, S.; Peluso, F.; Stefanile, M.; Pappone, G. Ancient Coastal Changes Due to Ground Movements and Human Interventions in the Roman Portus Julius (Pozzuoli Gulf, Italy): Results from Photogrammetric and Direct Surveys. *Water* **2020**, *12*, 658. [\[CrossRef\]](#)
14. Faivre, S.; Bakran-Petricoli, T.; Barešić, J.; Horvatić, D.; Macario, K. Relative Sea-Level Change and Climate Change in the Northeastern Adriatic during the Last 1.5 Ka (Istria, Croatia). *Quat. Sci. Rev.* **2019**, *222*, 105909. [\[CrossRef\]](#)
15. Evelpidou, N.; Melini, D.; Pirazzoli, P.; Vassilopoulos, A. Evidence of a Recent Rapid Subsidence in the S–E Cyclades (Greece): An Effect of the 1956 Amorgos Earthquake. *Cont. Shelf Res.* **2012**, *39–40*, 27–40. [\[CrossRef\]](#)
16. Evelpidou, N.; Karkani, A.; Kampolis, I. Relative Sea Level Changes and Morphotectonic Implications Triggered by the Samos Earthquake of 30th October 2020. *J. Mar. Sci. Eng.* **2021**, *9*, 40. [\[CrossRef\]](#)
17. Saitis, G.; Karkani, A.; Evelpidou, N.; Maroukian, H. Palaeogeographical Reconstruction of Ancient Diolkos Slipway by Using Beachrocks as Proxies, West Corinth Isthmus, Greece. *Quaternary* **2022**, *5*, 7. [\[CrossRef\]](#)
18. Khan, N.S.; Ashe, E.; Shaw, T.A.; Vacchi, M.; Walker, J.; Peltier, W.R.; Kopp, R.E.; Horton, B.P. Holocene Relative Sea-Level Changes from Near-, Intermediate-, and Far-Field Locations. *Curr. Clim. Chang. Rep.* **2015**, *1*, 247–262. [\[CrossRef\]](#)
19. Vacchi, M.; Marriner, N.; Morhange, C.; Spada, G.; Fontana, A.; Rovere, A. Multiproxy Assessment of Holocene Relative Sea-Level Changes in the Western Mediterranean: Sea-Level Variability and Improvements in the Definition of the Isostatic Signal. *Earth Sci. Rev.* **2016**, *155*, 172–197. [\[CrossRef\]](#)
20. Faivre, S.; Butorac, V. Recently Submerged Tidal Notches in the Wider Makarska Area (Central Adriatic, Croatia). *Quat. Int.* **2018**, *494*, 225–235. [\[CrossRef\]](#)
21. Marriner, N.; Morhange, C.; Faivre, S.; Flaux, C.; Vacchi, M.; Miko, S.; Dumas, V.; Boetto, G.; Radic Rossi, I. Post-Roman Sea-Level Changes on Pag Island (Adriatic Sea): Dating Croatia’s “Enigmatic” Coastal Notch. *Geomorphology* **2014**, *221*, 83–94. [\[CrossRef\]](#)
22. de Gelder, G.; Fernández-Blanco, D.; Melnick, D.; Duclaux, G.; Bell, R.E.; Jara-Muñoz, J.; Armijo, R.; Lacassin, R. Lithospheric Flexure and Rheology Determined by Climate Cycle Markers in the Corinth Rift. *Sci. Rep.* **2019**, *9*, 4260. [\[CrossRef\]](#)
23. Tsanakas, K.; Saitis, G.; Evelpidou, N.; Karymbalis, E.; Karkani, A. Late Pleistocene Geomorphic Evolution of Cephalonia Island, Western Greece, Inferred from Uplifted Marine Terraces. *Quaternary* **2022**, *5*, 35. [\[CrossRef\]](#)
24. Papanastassiou, D.; Cundy, A.B.; Gaki-Papanastassiou, K.; Frogley, M.R.; Tsanakas, K.; Maroukian, H. The Uplifted Terraces of the Arkitsa Region, NW Evoikos Gulf, Greece: A Result of Combined Tectonic and Volcanic Processes. *J. Geol.* **2014**, *122*, 397–410. [\[CrossRef\]](#)
25. Karymbalis, E.; Tsanakas, K.; Tsoudoulos, I.; Gaki-Papanastassiou, K.; Papanastassiou, D.; Batzakis, D.-V.; Stamoulis, K. Late Quaternary Marine Terraces and Tectonic Uplift Rates of the Broader Neapolis Area (SE Peloponnese, Greece). *J. Mar. Sci. Eng.* **2022**, *10*, 99. [\[CrossRef\]](#)
26. Cerrone, C.; Di Donato, V.; Mazzoli, S.; Robustelli, G.; Soligo, M.; Tuccimei, P.; Ascione, A. Development and Deformation of Marine Terraces: Constraints to the Evolution of the Campania Plain Quaternary Coastal Basin (Italy). *Geomorphology* **2021**, *385*, 107725. [\[CrossRef\]](#)
27. Polidorou, M.; Saitis, G.; Evelpidou, N. Beachrock Development as an Indicator of Paleogeographic Evolution, the Case of Akrotiri Peninsula, Cyprus. *Z. Geomorphol.* **2021**, *63*, 3–17. [\[CrossRef\]](#)
28. Karkani, A.; Evelpidou, N.; Vacchi, M.; Morhange, C.; Tsukamoto, S.; Frechen, M.; Maroukian, H. Tracking Shoreline Evolution in Central Cyclades (Greece) Using Beachrocks. *Mar. Geol.* **2017**, *388*, 25–37. [\[CrossRef\]](#)
29. Mauz, B.; Vacchi, M.; Green, A.; Hoffmann, G.; Cooper, A. Beachrock: A Tool for Reconstructing Relative Sea Level in the Far-Field. *Mar. Geol.* **2015**, *362*, 1–16. [\[CrossRef\]](#)
30. Vacchi, M. Assessing the Late Quaternary Coastal Uplift of Lesvos Island Using Beachrocks Distribution and Morphology. *Quat. Int.* **2012**, *279–280*, 509. [\[CrossRef\]](#)
31. Alexandrakis, G.; Petrakis, S.; Kampanis, N.A. Integrating Geomorphological Data, Geochronology and Archaeological Evidence for Coastal Landscape Reconstruction, the Case of Ammoudara Beach, Crete. *Water* **2021**, *13*, 1269. [\[CrossRef\]](#)
32. Vacchi, M.; Russo Ermolli, E.; Morhange, C.; Ruello, M.R.; Di Donato, V.; Di Vito, M.A.; Giampaola, D.; Carsana, V.; Liuzza, V.; Cinque, A.; et al. Millennial Variability of Rates of Sea-Level Rise in the Ancient Harbour of Naples (Italy, Western Mediterranean Sea). *Quat. Res.* **2020**, *93*, 284–298. [\[CrossRef\]](#)
33. Laborel, J.; Laborel-Deguen, F. Biological Indicators of Holocene Sea-Level and Climatic Variations on Rocky Coasts of Tropical and Subtropical Regions. *Quat. Int.* **1996**, *31*, 53–60. [\[CrossRef\]](#)

34. Hibbert, F.D.; Williams, F.H.; Fallon, S.J.; Rohling, E.J. A Database of Biological and Geomorphological Sea-Level Markers from the Last Glacial Maximum to Present. *Sci. Data* **2018**, *5*, 180088. [[CrossRef](#)] [[PubMed](#)]
35. Faivre, S.; Bakran-Petricioli, T.; Barešić, J.; Horvatić, D. Lithophyllum Rims as Biological Markers for Constraining Palaeoseismic Events and Relative Sea-Level Variations during the Last 3.3 Ka on Lopud Island, Southern Adriatic, Croatia. *Glob. Planet. Chang.* **2021**, *202*, 103517. [[CrossRef](#)]
36. Rovere, A.; Antonioli, F.; Bianchi, C.N. Fixed Biological Indicators. In *Handbook of Sea-Level Research*; Shennan, I., Long, A.J., Horton, B.P., Eds.; John Wiley & Sons, Ltd.: Hoboken, NJ, USA, 2015; pp. 268–280. ISBN 978-1-118-45258-5.
37. Bechor, B.; Theodoulou, T.; Spada, G.; Dean, S.; Sivan, D. Medieval Relative Low Sea-Level Indications from the Peloponnese and the Aegean Sea. *Quat. Int.* **2020**, *545*, 17–27. [[CrossRef](#)]
38. Evelpidou, N.; Karkani, A. Archaeology and Sea-Level Change. In *Encyclopedia of Coastal Science*; Finkl, C., Makowski, C., Eds.; Springer: Cham, Switzerland, 2018; ISBN 9783319486574.
39. Auriemma, R.; Solinas, E. Archaeological Remains as Sea Level Change Markers: A Review. *Quat. Int.* **2009**, *206*, 134–146. [[CrossRef](#)]
40. Melis, R.T.; Di Rita, F.; French, C.; Marriner, N.; Montis, F.; Serreli, G.; Sulas, F.; Vacchi, M. 8000 Years of Coastal Changes on a Western Mediterranean Island: A Multiproxy Approach from the Posada Plain of Sardinia. *Mar. Geol.* **2018**, *403*, 93–108. [[CrossRef](#)]
41. Karkani, A.; Evelpidou, N.; Giaime, M.; Marriner, N.; Morhange, C.; Spada, G. Late Holocene Sea-Level Evolution of Paros Island (Cyclades, Greece). *Quat. Int.* **2019**, *500*, 139–146. [[CrossRef](#)]
42. Karymbalis, E.; Tsanakas, K.; Cundy, A.; Iliopoulos, G.; Papadopoulou, P.; Protopappas, D.; Gaki-Papanastassiou, K.; Papanastassiou, D.; Batzakis, D.V.; Kotinas, V.; et al. Late Holocene Palaeogeographic Evolution of the Lihoura Coastal Plain, Pteleos Gulf, Central Greece. *Quat. Int.* **2022**, *638–639*, 70–83. [[CrossRef](#)]
43. D'Orefice, M.; Bellotti, P.; Bertini, A.; Calderoni, G.; Neri, P.C.; Di Bella, L.; Fiorenza, D.; Foresi, L.M.; Louvari, M.A.; Rainone, L.; et al. Holocene Evolution of the Burano Paleo-Lagoon (Southern Tuscany, Italy). *Water* **2020**, *12*, 1007. [[CrossRef](#)]
44. Mattei, G.; Caporizzo, C.; Corrado, G.; Vacchi, M.; Stocchi, P.; Pappone, G.; Schiattarella, M.; Aucelli, P.P.C. On the Influence of Vertical Ground Movements on Late-Quaternary Sea-Level Records. A Comprehensive Assessment along the Mid-Tyrrhenian Coast of Italy (Mediterranean Sea). *Quat. Sci. Rev.* **2022**, *279*, 107384. [[CrossRef](#)]
45. Distefano, S.; Gamberi, F.; Borzi, L.; Di Stefano, A. Quaternary Coastal Landscape Evolution and Sea-Level Rise: An Example from South-East Sicily. *Geosciences* **2021**, *11*, 506. [[CrossRef](#)]
46. Distefano, S.; Gamberi, F.; Baldassini, N.; Di Stefano, A. Quaternary Evolution of Coastal Plain in Response to Sea-Level Changes: Example from South-East Sicily (Southern Italy). *Water* **2021**, *13*, 1524. [[CrossRef](#)]
47. Briole, P.; Rigo, A.; Lyon-Caen, H.; Ruegg, J.C.; Papazissi, K.; Mitsakaki, C.; Balodimou, A.; Veis, G.; Hatzfeld, D.; Deschamps, A. Active Deformation of the Corinth Rift, Greece: Results from Repeated Global Positioning System Surveys between 1990 and 1995. *J. Geophys. Res. Solid Earth* **2000**, *105*, 25605–25625. [[CrossRef](#)]
48. Reilinger, R.; McClusky, S.; Paradissis, D.; Ergintav, S.; Vernant, P. Geodetic Constraints on the Tectonic Evolution of the Aegean Region and Strain Accumulation along the Hellenic Subduction Zone. *Tectonophysics* **2010**, *488*, 22–30. [[CrossRef](#)]
49. Vassilakis, E.; Royden, L.; Papanikolaou, D. Kinematic Links between Subduction along the Hellenic Trench and Extension in the Gulf of Corinth, Greece: A Multidisciplinary Analysis. *Earth Planet. Sci. Lett.* **2011**, *303*, 108–120. [[CrossRef](#)]
50. Jackson, J.A.; Gagnepain, J.; Houseman, G.; King, G.C.P.; Papadimitriou, P.; Soufleris, C.; Virieux, J. Seismicity, Normal Faulting, and the Geomorphological Development of the Gulf of Corinth (Greece): The Corinth Earthquakes of February and March 1981. *Earth Planet. Sci. Lett.* **1982**, *57*, 377–397. [[CrossRef](#)]
51. Hubert, A.; King, G.; Armijo, R.; Meyer, B.; Papanastassiou, D. Fault Re-Activation, Stress Interaction and Rupture Propagation of the 1981 Corinth Earthquake Sequence. *Earth Planet. Sci. Lett.* **1996**, *142*, 573–585. [[CrossRef](#)]
52. Morewood, N.C.; Roberts, G.P. Comparison of Surface Slip and Focal Mechanism Slip Data along Normal Faults: An Example from the Eastern Gulf of Corinth, Greece. *J. Struct. Geol.* **2001**, *23*, 473–487. [[CrossRef](#)]
53. Roberts, G.P. Variation in Fault-Slip Directions along Active and Segmented Normal Fault Systems. *J. Struct. Geol.* **1996**, *18*, 835–845. [[CrossRef](#)]
54. Stuiver, M.; Reimer, P.J.; Reimer, R.W. CALIB 7.1 [WWW Program]. Available online: <http://calib.org> (accessed on 9 August 2020).
55. Heaton, T.J.; Köhler, P.; Butzin, M.; Bard, E.; Reimer, R.W.; Austin, W.E.N.; Bronk Ramsey, C.; Grootes, P.M.; Hughen, K.A.; Kromer, B.; et al. Marine20—The Marine Radiocarbon Age Calibration Curve (0–55,000 Cal BP). *Radiocarbon* **2020**, *62*, 779–820. [[CrossRef](#)]
56. Reimer, P.J.; McCormac, F.G. Marine Radiocarbon Reservoir Correction for the Mediterranean and Aegean Seas. *Radiocarbon* **2002**, *44*, 159–166. [[CrossRef](#)]
57. Vacchi, M.; Rovere, A.; Zouros, N.; Desruelles, S.; Caron, V.; Firpo, M. Spatial Distribution of Sea-Level Markers on Lesbos Island (NE Aegean Sea): Evidence of Differential Relative Sea-Level Changes and the Neotectonic Implications. *Geomorphology* **2012**, *159–160*, 50–62. [[CrossRef](#)]
58. Hijma, M.P.; Engelhart, S.E.; Törnqvist, T.E.; Horton, B.P.; Hu, P.; Hill, D.F. A Protocol for a Geological Sea-Level Database. In *Handbook of Sea-Level Research*; John Wiley & Sons, Ltd.: Hoboken, NJ, USA, 2015; pp. 536–553. ISBN 9781118452547.

59. Khan, N.S.; Horton, B.P.; Engelhart, S.; Rovere, A.; Vacchi, M.; Ashe, E.L.; Törnqvist, T.E.; Dutton, A.; Hijma, M.P.; Shennan, I. Inception of a Global Atlas of Sea Levels since the Last Glacial Maximum. *Quat. Sci. Rev.* **2019**, *220*, 359–371. [[CrossRef](#)]
60. Vacchi, M.; Ghilardi, M.; Spada, G.; Currás, A.; Robresco, S. New Insights into the Sea-Level Evolution in Corsica (NW Mediterranean) since the Late Neolithic. *J. Archaeol. Sci. Rep.* **2017**, *12*, 782–793. [[CrossRef](#)]
61. Fontana, A.; Vinci, G.; Tasca, G.; Mozzi, P.; Vacchi, M.; Bivi, G.; Salvador, S.; Rossato, S.; Antonioli, F.; Asioli, A.; et al. Lagoonal Settlements and Relative Sea Level during Bronze Age in Northern Adriatic: Geoarchaeological Evidence and Paleogeographic Constraints. *Quat. Int.* **2017**, *439*, 17–36. [[CrossRef](#)]
62. Roberts, G.; Papanikolaou, I.D.; Vott, A.; Pantosti, D.; Hadler, H. Active Tectonics and Earthquake Geology of the Perachora Peninsula and the Area of the Isthmus, Corinth Gulf, Greece. In *Field Trip Guide; The Natural Hazards Laboratory: Athens, Greece, 2011*; ISBN 978-960-466-094-0.
63. Roberts, G.P.; Houghton, S.L.; Underwood, C.; Papanikolaou, I.; Cowie, P.A.; van Calsteren, P.; Wigley, T.; Cooper, F.J.; McArthur, J.M. Localization of Quaternary Slip Rates in an Active Rift in 10 5 Years: An Example from Central Greece Constrained by 234U-230Th Coral Dates from Uplifted Paleoshorelines. *J. Geophys. Res.* **2009**, *114*, B10406. [[CrossRef](#)]
64. Mariolakos, I.; Papanikolaou, D.; Symeonidis, N.; Lekkas, S.; Karotsieris, Z.; Sideris, C. The Deformation of the Area around the Eastern Korinthian Gulf, Affected by the Earthquakes of February–March 1981. In Proceedings of the International Symposium on the Hellenic Arc and Trench (H.E.A.T.), Athens, Greece, 8–10 April 1982; pp. 400–420.
65. Khoury, S.G.; Tilford, N.R.; Chandra, U.; Amick, D. The Effect of Multiple Events on Isoseismal Maps of the 1981 Earthquakes at the Gulf of Corinth, Greece. *Bull. Seismol. Soc. Am.* **1983**, *73*, 655–660. [[CrossRef](#)]
66. Vita-Finzi, C.; King, G.C.P. The Seismicity, Geomorphology and Structural Evolution of the Corinth Area of Greece. *Philos. Trans. R. Soc. London* **1985**, *314*, 379–407.
67. Perissoratis, C.; Mitropoulos, D.; Angelopoulos, I. The Role of Earthquakes in Inducing Sediment Mass Movements in the Eastern Korinthiakos Gulf. An Example from the February 24–March 4, 1981 Activity. *Mar. Geol.* **1984**, *55*, 35–45. [[CrossRef](#)]
68. Bentham, P.; Collier, R.; Gawthorpe, R.L.; Leeder, M.R.; Prossor, S.; Stark, C. Tectono-Sedimentary Development of an Extensional Basin: The Neogene Megara Basin, Greece. *J. Geol. Soc. Lond.* **1991**, *148*, 923–934. [[CrossRef](#)]
69. Collier, R.E.L.; Leeder, M.R.; Rowe, P.J.; Atkinson, T.C. Rates of Tectonic Uplift in the Corinth and Megara Basins, Central Greece. *Tectonics* **1992**, *11*, 1159–1167. [[CrossRef](#)]
70. Leeder, M.R.; Portman, C.; Andrews, J.E.; Collier, R.E.L.; Finch, E.; Gawthorpe, R.L.; McNeill, L.C.; Pérez-Arlucea, M.; Rowe, P. Normal Faulting and Crustal Deformation, Alkyonides Gulf and Perachora Peninsula, Eastern Gulf of Corinth Rift, Greece. *J. Geol. Soc. Lond.* **2005**, *162*, 549–561. [[CrossRef](#)]
71. Kelletat, D. Beachrock as Sea-Level Indicator? Remarks from a Geomorphological Point of View. *J. Coast. Res.* **2006**, *226*, 1558–1564. [[CrossRef](#)]
72. Voudoukas, M.I.; Velegrakis, A.F.; Plomaritis, T.A. Beachrock Occurrence, Characteristics, Formation Mechanisms and Impacts. *Earth Sci. Rev.* **2007**, *85*, 23–46. [[CrossRef](#)]
73. Rieradevall, M.; Roca, J.R. Distribution and Population Dynamics of Ostracodes (Crustacea, Ostracoda) in a Karstic Lake: Lake Banyoles (Catalonia, Spain). *Hydrobiologia* **1995**, *310*, 189–196. [[CrossRef](#)]
74. Ruiz, F.; Abad, M.; Bodergat, A.M.; Carbonel, P.; Rodríguez-Lázaro, J.; González-Regalado, M.L.; Toscano, A.; García, E.X.; Prenda, J. Freshwater Ostracods as Environmental Tracers. *Int. J. Environ. Sci. Technol.* **2013**, *10*, 1115–1128. [[CrossRef](#)]
75. Gaki-Papanastassiou, K.; Karymbalis, E.; Papanastassiou, D.; Maroukian, H. Quaternary Marine Terraces as Indicators of Neotectonic Activity of the Ierapetra Normal Fault SE Crete (Greece). *Geomorphology* **2009**, *104*, 38–46. [[CrossRef](#)]
76. Lambeck, K.; Purcell, A. Sea-Level Change in the Mediterranean Sea since the LGM: Model Predictions for Tectonically Stable Areas. *Quat. Sci. Rev.* **2005**, *24*, 1969–1988. [[CrossRef](#)]

**Disclaimer/Publisher’s Note:** The statements, opinions and data contained in all publications are solely those of the individual author(s) and contributor(s) and not of MDPI and/or the editor(s). MDPI and/or the editor(s) disclaim responsibility for any injury to people or property resulting from any ideas, methods, instructions or products referred to in the content.